Scattering attenuation ratios of *P* and *S* waves in elastic media

Tae-Kyung Hong*

Research School of Earth Sciences, Institute of Advanced Studies, The Australian National University, Canberra, ACT 0200, *Australia.*
E-mail: tkhong@es.ucsc.edu

SUMMARY

The variation of scattering attenuation ratios of *P* and *S* waves (Q_P^{-1}/Q_S^{-1}) is investigated in elastic media by using numerical simulations and theoretical expressions based on the first-order Born approximation. Numerical results from stochastic random media (von Karman, exponential, Gaussian) with mild velocity perturbation (10 per cent in this study) are represented well by theoretical attenuation curves with a minimum scattering angle of 60–90°. The level of scattering attenuation ratios is dependent on the velocity ratio ($\gamma = \alpha_0/\beta_0$) and the type of medium. The change of perturbation in the density introduces a relatively small variation in attenuation ratio. Attenuation ratios are proportional to normalized frequency (*fa*, frequency-by-correlation length) at the intermediate-frequency range ($0.1 \text{ km s}^{-1} < fa < 10 \text{ km s}^{-1}$) and determined constant at the high-frequency ($fa > 10 \text{ km s}^{-1}$) and low-frequency ($fa < 1 \text{ km s}^{-1}$) regimes. The von Karman-type models look appropriate for the representation of small-scale variation in the Earth. The scattering attenuation ratios can be implemented for the investigation of small-scale heterogeneities in the Earth.

Key words: attenuation, elastic waves, numerical modelling, scattering, wavelet-based method, wavelets.

GJI Seismology

1 INTRODUCTION

Seismic attenuation is a well-known feature associated with wave propagation in the Earth, and much work based on field data has been done to resolve the strength of apparent attenuation in various areas (e.g. Hatzidimitriou 1995; Tselentis 1998; Yoshimoto *et al.* 1998; Adams & Abercrombie 1998; Chung & Sato 2001).

Total attenuation rates are determined as the sum of scattering (Q_s^{-1}) and intrinsic attenuations (Q_i^{-1}). It was reported, however, that scattering attenuation is generally the dominant factor in seismic attenuation in the crust (e.g. Hatzidimitriou 1994; Del Pezzo *et al.* 1995). Also, even when the intrinsic attenuation is comparable to the scattering attenuation, the intrinsic attenuation appears to vary with the scattering attenuation (e.g. Mayeda *et al.* 1992). Thus, investigation of scattering attenuation will allow us to understand seismic attenuation patterns in the crust.

Stochastic random heterogeneities have been implemented widely for the investigation of heterogeneities in the Earth (e.g. Hedlin & Shearer 2002). However, it is not resolved clearly which type of stochastic random model is appropriate for the representation of small-scale variation in global structure. The type of medium may be varied with the physical and chemical environment. Thus, it is required to determine the type of medium considering the signature found in seismic responses. There have been several trials to characterize media in terms of stochastic heterogeneities using amplitude and phase fluctuation (e.g. Line *et al.* 1998). However, the amplitude and phase fluctuations are highly dependent on the propagation path, and the measured results display a different pattern following the appearance of the media (Hong *et al.* 2003). An alternative way to characterize media in terms of stochastic random heterogeneities could be to use scattering attenuation ratios of *P* and *S* waves (Q_P^{-1}/Q_S^{-1}) which involve information from both *P* and *S* waves. For this purpose, it is necessary to resolve the properties of scattering attenuation ratios in the stochastic random model.

Although the ultimate goal is to understand scattering in 3-D, we are able to use 2-D waves and structures since 3-D scattering effects are so close to 2-D (Frenje & Juhlin 2000); also the 2-D simulations have a greater advantage in analysis, such as saving computational resources in numerical modelling and easy assessment of scattering energy during wave-type coupling. In fact, the theoretical expressions for attenuation in 3-D (Sato & Fehler 1998) require 3-D integrations, resulting in multiple 2-D integrations, over propagation angles to describe

*Now at: Earth Sciences Department/IGPP, University of California, Santa Cruz, USA.

the dependence of coupled phases (i.e. *SP, PS*) on the scattering angle due to the geometrical complexity of heterogeneities. The corresponding expressions are much simpler in 2-D and can be readily compared with numerical results. Although the absolute magnitude of energy losses due to scattering may be different between 2-D and 3-D cases, the scattering attenuation ratios are expected to be consistent between both cases.

A theoretical expression for scattering attenuation for comparison with experimental results can be formulated by considering the single scattering approximation (first-order Born approximation, Sato 1982; Wu 1982). This scattering attenuation formulation, however, requires a correction for the forward scattering effect which increases apparent attenuation by the introduction of a traveltime anomaly in time responses. The apparent attenuation can be corrected by excluding the contribution of the forward scattered energy from the entire scattered energy. The cone inside a specific angle is regarded as the region influenced by the forward scattering waves. Here, the specific angle is measured from the direction of incidence and is called the minimum (or cut-off) scattering angle.

It is, therefore, important to determine the minimum scattering angle correctly for the implementation of theoretical expressions in seismic quantitative studies. Various studies have been done to resolve the minimum scattering angles in acoustic (e.g. Jannaud *et al.* 1991; Roth & Korn 1993; Frenje & Juhlin 2000) and elastic media (e.g. Frankel & Clayton 1986; Fang & Müller 1996). Many previous studies on elastic waves, however, implemented the theoretical expressions for scalar (or acoustic) waves, so the minimum scattering angle of elastic waves could not be resolved properly. Recently, Hong & Kennett (2003a) formulated the theoretical 2-D scattering attenuation variation for *P* waves, and showed that theoretical curves with a minimum scattering angle of 60–90° well represent the results from mildly perturbed media (10 per cent velocity perturbation). However, the companion for 2-D *S* waves has not been formulated yet, and its minimum scattering angle remains unknown.

In order to correctly assess from time responses the energy loss due to scattering, a numerical modelling technique with high accuracy is obviously desired. In fact, it has been reported that artificial attenuation can be incorporated during numerical modelling due to limitation in spatial differentiations of the accuracy of the wavefield in perturbed media (Hong & Kennett 2003a). In this study we implement a wavelet-based method (Hong & Kennett 2002a,b, 2003b) which retains high accuracy and stability even in highly heterogeneous media.

We validate the theoretical expressions for scattering attenuation for *S* waves by comparison with numerical results in four different types of stochastic random models: von Karman with Hurst number $\nu = 0.05$ and 0.25, exponential and Gaussian random media. Also the corresponding minimum scattering angle is resolved. Then the scattering attenuation ratios of *P* and *S* waves are investigated in terms of frequency by implementing the validated theoretical expressions for attenuation. The estimated attenuation ratios from the stochastic random media are interpreted in terms of the scattering properties of elastic waves by considering field observations.

2 THEORETICAL FORMULATION OF SCATTERING ATTENUATION

The 2-D theoretical scattering attenuation of *P* waves, based on the first-order Born approximation, can be formulated as a function of a normalized wavenumber $k_\alpha a$ (Hong & Kennett 2003a):

$$
\frac{Q_P^{-1}}{\epsilon^2} = \frac{k_\alpha^2}{8\pi} \int_{\theta_{\min}^{PP}}^{2\pi - \theta_{\min}^{PP}} \left[C_{\mathrm{r}}^P(\theta)\right]^2 \mathcal{P}\left(2k_\alpha \sin\frac{\theta}{2}\right) d\theta
$$

$$
+ \frac{k_\alpha^2 \gamma^2}{8\pi} \int_{\theta_{\min}^{PS}}^{2\pi - \theta_{\min}^{PS}} \left[C_{\mathrm{t}}^P(\theta)\right]^2 \mathcal{P}\left(k_\alpha\sqrt{1 + \gamma^2 - 2\gamma\cos\theta}\right) d\theta, \tag{1}
$$

where γ is the ratio of *P* and *S* wave velocities in the background media ($=\alpha_0/\beta_0$), k_α is the wavenumber of the incident *P* waves, *a* is the correlation length of stochastic random heterogeneities, θ is the angle between the propagation directions of incident and scattered waves and $\mathcal{P}$ is the power spectral density function of stochastic random media. The coefficients $C_{\mathrm{r}}^P(\theta)$ and $C_{\mathrm{t}}^P(\theta)$ are

$$
C_{\mathrm{r}}^P(\theta) = \sin\theta \left[C_1^P A_{11}^P(\theta)\sin\theta + 2A_{12}^P(\theta) + C_2^P A_{12}^P(\theta)(\cos\theta - 1)\right]
$$

$$
+ \cos\theta \left[C_1^P A_{21}^P(\theta)\sin\theta + 2A_{22}^P(\theta) + C_2^P A_{22}^P(\theta)(\cos\theta - 1)\right],
$$

$$
C_{\mathrm{t}}^P(\theta) = \cos\theta \left[C_1^P A_{11}^S(\theta)\gamma\sin\theta + 2A_{12}^S(\theta) + C_2^P A_{12}^S(\theta)(\gamma\cos\theta - 1)\right]
$$

$$
- \sin\theta \left[C_1^P A_{21}^S(\theta)\gamma\sin\theta + 2A_{22}^S(\theta) + C_2^P A_{22}^S(\theta)(\gamma\cos\theta - 1)\right], \tag{2}
$$

and C_1^P and C_2^P are

$$
C_1^P = (K + 2)\left(1 - \frac{2}{\gamma^2}\right), \quad C_2^P = K + 2. \tag{3}
$$

Here, *K* is a constant for the strength of the density perturbation. The minimum scattering angles for coupled scattered waves ($\theta_{\min}^{PS}$) can be determined in those terms for in-phase scattered waves ($\theta_{\min}^{PP}$):

$$
\theta_{\min}^{PS} = \theta_{\min}^{PP} + (\psi_P - \psi_S), \quad \psi_P = \frac{\pi - \theta_{\min}^{PP}}{2}, \quad \psi_S = \sin^{-1}\left(\frac{\sin\psi_P}{\gamma}\right), \tag{4}
$$

and A_{ij}^k $(i, j = 1, 2, k = P, S)$ is given by

$$A_{11}^P(\theta) = \sin^2\theta, \quad A_{12}^P(\theta) = \sin\theta\cos\theta, \quad A_{21}^P(\theta) = -\sin\theta\cos\theta, \quad A_{22}^P(\theta) = \cos^2\theta,$$

$$A_{11}^S(\theta) = \cos^2\theta, \quad A_{12}^S(\theta) = -\sin\theta\cos\theta, \quad A_{21}^S(\theta) = \sin\theta\cos\theta, \quad A_{22}^S(\theta) = \sin^2\theta.$$

(5)

Following the derivation procedure of the theoretical scattering attenuation expression for P waves in Hong & Kennett (2003a), the theoretical expression for S waves can be derived as

$$\frac{Q_S^{-1}}{\epsilon^2} = \frac{k_\beta^2}{8\pi\gamma^4} \int_{\theta_{min}^{SP}}^{2\pi-\theta_{min}^{SP}} \left[C_r^S(\theta)\right]^2 \mathcal{P}\left(\frac{k_\beta}{\gamma}\sqrt{1+\gamma^2-2\gamma\cos\theta}\right) d\theta$$

$$+ \frac{k_\beta^2}{8\pi} \int_{\theta_{min}^{SS}}^{2\pi-\theta_{min}^{SS}} \left[C_t^S(\theta)\right]^2 \mathcal{P}\left(2k_\beta\sin\frac{\theta}{2}\right) d\theta,$$

(6)

where k_β is the wavenumber of S waves, and the minimum scattering angles $(\theta_{min}^{SS}, \theta_{min}^{SP})$ for in-phase scattered waves (SS) and wave type-coupled phase (SP) are given by

$$\theta_{min}^{SP} = \theta_{min}^{SS} - (\phi_P - \phi_S), \quad \phi_S = \frac{\pi - \theta_{min}^{SS}}{2}, \quad \phi_P = \sin^{-1}(\gamma\sin\phi_S).$$

(7)

Here, the coefficients C_r^S and C_t^S are

$$C_r^S(\theta) = \sin\theta\left[-\gamma C_1^S A_{11}^P(\theta) + (\cos\theta - \gamma)C_2^S A_{11}^P(\theta) + \sin\theta C_2^S A_{12}^P(\theta)\right]$$

$$+ \cos\theta\left[-\gamma C_1^S A_{21}^P(\theta) + (\cos\theta - \gamma)C_2^S A_{21}^P(\theta) + \sin\theta C_2^S A_{22}^P(\theta)\right],$$

$$C_t^S(\theta) = \cos\theta\left[-C_1^S A_{11}^S(\theta) + (\cos\theta - 1)C_2^S A_{11}^S(\theta) + \sin\theta C_2^S A_{12}^S(\theta)\right]$$

$$- \sin\theta\left[-C_1^S A_{21}^S(\theta) + (\cos\theta - 1)C_2^S A_{21}^S(\theta) + \sin\theta C_2^S A_{22}^S(\theta)\right],$$

(8)

where $C_1^S = -2$ and $C_2^S = K + 2$. Details of the derivation are given in Appendix A.

Note that the theoretical expressions for attenuation (eqs 1 and 6) were derived with consideration of the empirical relationship of physical parameters in the Earth (e.g. Shiomi *et al.* 1997; Sato & Fehler 1998), in which the perturbations of wave velocities and density are linearly correlated. Thus the perturbations of wave velocities and density can be represented simply in terms of a spatial perturbation function $\xi(x, z)$:

$$\xi(x, z) = \frac{\delta\alpha}{\alpha_0} = \frac{\delta\beta}{\beta_0} = \frac{1}{K}\frac{\delta\rho}{\rho_0},$$

(9)

where ρ_0 is the density of the background medium and K is the constant in eq. (3) which controls the strength of density perturbation.

Since in-phase forward scattered waves are mainly responsible for the apparent attenuation by traveltime anomaly, it is useful to consider the minimum scattering angles in terms of the in-phase scattering angles, i.e. θ_{min}^{PP} for P-wave and θ_{min}^{SS} for S-wave scattering problems. The scattered waves in wave-type coupled phases $(PS$ and $SP)$ also play a role in the traveltime anomaly in a physical experiment since random heterogeneities are not present in discrete form as assumed in the theory. Thus, the influence of the coupled phases should be considered, and their scattering angle $(\theta_{min}^{PS}, \theta_{min}^{SP})$ can be expressed simply in terms of the scattering angles for in-phase waves $(\theta_{min}^{PP}, \theta_{min}^{SS})$ using Snell's law. It is noteworthy that the scattering angles of in-phase waves are held constant for changes in the velocity ratios (γ) of media, while those for coupled phases vary with γ. The consideration of the minimum scattering angles for coupled phases may not be sufficient in highly perturbed media due to the multiscattering effect. However, in the context of weak perturbation on which the single scattering theory is based, the consideration of scattering angles in terms of the in-phase angles is adequate for analysis.

3 COMPARISON OF THEORETICAL RATES WITH RESULTS FROM NUMERICAL MODELLING

The theoretical expression for attenuation of P waves was formulated and compared with results from numerical modelling in representative stochastic random media (Hong & Kennett 2003a). The attenuation rates from numerical modelling in random media with 10 per cent velocity perturbation are well represented by theoretical curves with a minimum scattering angle (θ_{min}^{PP}) of 60–90°. Before we proceed to the investigation of scattering attenuation ratios (Q_P^{-1}/Q_S^{-1}) with the aid of the theoretical expressions, we determine the representative theoretical curve for shear waves.

Stochastic random models are constructed through 2-D Fourier transforms of the power spectral density function (PSDF, $\mathcal{P}(k)$) with random phase $\Phi(k_x, k_z)$ varying between $-\pi$ and π. The random phase is assigned to the 2-D wavenumber gridpoints (k_x, k_z). Here the PSDF is the spectrum of the autocorrelation function (ACF, $N(r)$). We refer to Roth & Korn (1993) and Hong & Kennett (2003a) for details of the construction of random media.

We consider von Karman, exponential and Gaussian random media. The von Karman ACF and PSDF in 2-D media are (Sato & Fehler 1998)

$$N(r) = \frac{1}{2^{\nu-1}\Gamma(\nu)}\left(\frac{r}{a}\right)^\nu K_\nu\left(\frac{r}{a}\right), \quad \mathcal{P}(k) = \frac{4\pi\nu a^2}{(1+k^2a^2)^{\nu+1}},$$

(10)

where r is the spatial lag, a is the correlation distance, ν is the Hurst number, Γ is the gamma function, k is a wavenumber and K_ν is the modified Bessel function of order ν. The exponential ACF and PSDF are

$$N(r) = \mathrm{e}^{-r/a}, \quad \mathcal{P}(k) = \frac{2\pi a^2}{(1 + k^2 a^2)^{3/2}}. \tag{11}$$

Note that the exponential ACF is identical to the von Karman ACF with $\nu = 0.5$. The final model, Gaussian random media, is given by

$$N(r) = \mathrm{e}^{-r^2/a^2}, \quad \mathcal{P}(k) = \pi a^2 \mathrm{e}^{-k^2 a^2/4}. \tag{12}$$

Fig. 1 displays the textures of stochastic random media with a correlation distance of 214.5 m. In von Karman type models, high-frequency texture is reduced and transition in velocity perturbation becomes smooth with an increase in the Hurst number (ν). On the other hand, the texture of Gaussian media comprises low-frequency structures with a smooth transition.

We perform numerical modelling using a wavelet-based method (Hong & Kennett 2002a,b, 2003b) which generates accurate and stable results even in highly perturbed media (Hong & Kennett 2003a). Three different scales of heterogeneities with autocorrelation distance $a = 214.5$, 538.7 and 1353.2 m are considered for each stochastic random model (von Karman random media with Hurst number $\nu = 0.05$ and 0.25, exponential and Gaussian random media). Here each random model is realized in four different appearances using different random seeds, and the results from the four differently realized models are compared with each other to show the consistency in the numerical results.

The size of the medium is 19.3 by 77 km, and the spatial domain is represented by 128 by 512 gridpoints. Random heterogeneities with 10 per cent velocity perturbation and 8 per cent density perturbation (i.e. $K = 0.8$ in eq. 9) are added to a homogeneous medium with a P-wave velocity (α_0) of 6.738 km s^{-1}, an S-wave velocity (β_0) of 3.85 km s^{-1} and a density (ρ_0) of 2.9 g cm^{-3}. The top (Γ_{T}) and the bottom (Γ_{B}) boundaries are treated by absorbing boundary conditions, and the right (Γ_{R}) and the left (Γ_{L}) boundaries have periodic boundary
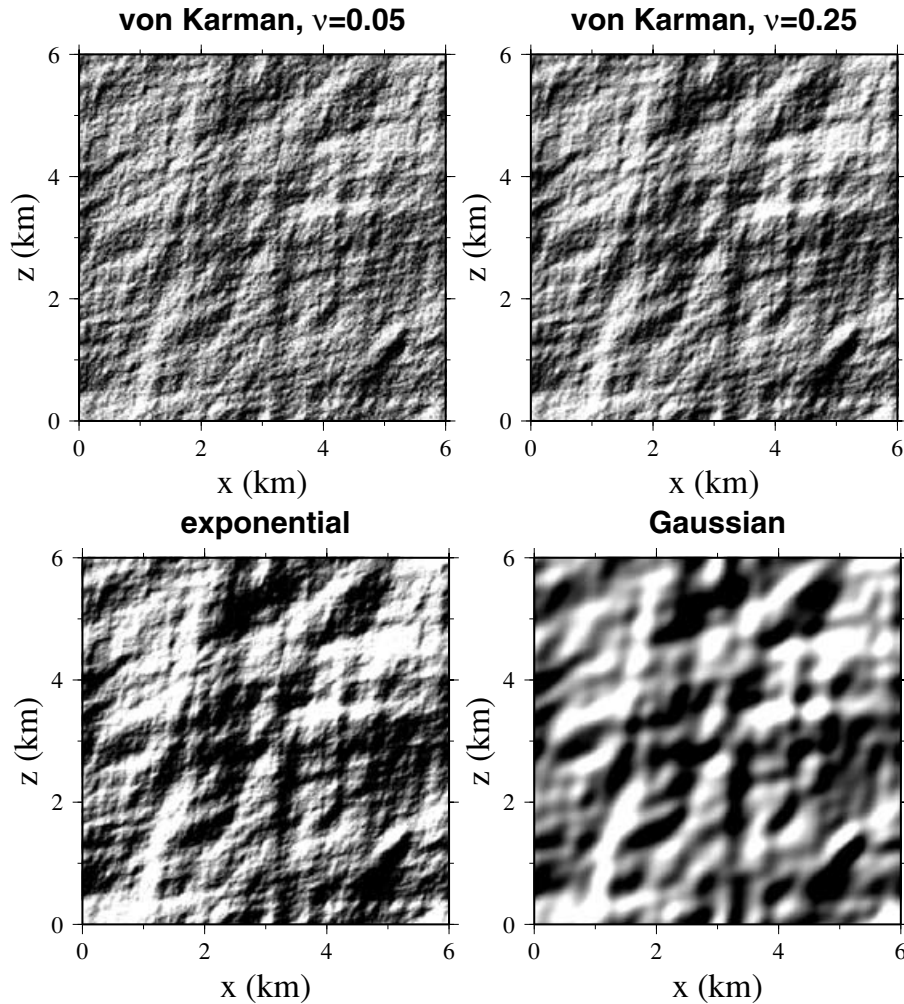

Figure 1. Normalized velocity perturbation in stochastic random media (von Karman with $\nu = 0.05$ and 0.25, exponential, Gaussian) with a correlation distance of 214.5 m. The strength of perturbation is represented by a black and white scale. The white represents a positive velocity anomaly and the black a negative velocity anomaly. As the Hurst number increases, the perturbation changes smoothly in von Karman type media; textures in a von Karman medium with small Hurst numbers display relatively high-frequency variations, while those with large Hurst numbers show low-frequency variations. The Gaussian medium displays extremely smooth variations for the perturbation.

conditions to suppress artificially reflected waves. Physically, the implementation of the periodic boundary conditions represents a case where unlimited plane waves are incident in unbounded random media. One hundred and twenty-eight receivers with a uniform interval of 150 m are deployed in a row at a distance of 55.9 km from the plane wave source. The locations of the receivers and the source in the domain are chosen at 10.5 km below the top boundary and above the bottom boundary so that the primary wavefields are not contaminated by spurious waves from absorbing boundaries. The Ricker wavelet with dominant frequency (f_d) of 4.5 Hz is used for the source–time function, and so the corresponding normalized wavenumbers for the dominant frequency ($k_\beta^d a$) are 1.58, 3.96 and 9.94.

Scattering attenuation rates are measured using spectral amplitudes of time responses (Aki & Richards 1980):

$$Q^{-1}(\omega) = \frac{2\beta_0}{\omega r} \ln\left(\frac{A_0(\omega)}{A_r(\omega)}\right), \tag{13}$$

where β_0 is the velocity of the incident wave, r is the spatial lag, ω is the angular frequency and $A_0(\omega)$ and $A_r(\omega)$ are spectral amplitudes of waves at the origin and at the receiver. The spectral amplitude of transmitted primary waves ($A_r(\omega)$) is computed by stacking all spectral amplitudes of time responses. Here, the time responses are tapered adaptively for wave trains before and after the primary-wave portion to exclude scattered waves before the stacking procedure in the Fourier domain. Considering the dominant frequency of incident waves, the spectral amplitudes at a frequency range of 2–10 Hz are implemented for the measurement of scattering attenuation in this study. It is noteworthy that Shapiro & Kneib (1993) indicated that attenuation rates can be determined differently according to the analysis procedure. For instance, they showed that the attenuation rates can be varied by a factor of 2 by exchanging the sequence of the stacking procedure and the logarithm of the amplitude ratio, and this phenomenon is obvious mathematically. The stacking process implemented in this study is considered with the idea that the mean stacked response stands for all time records and incorporates all the effect present in the time records. This idea has been implemented for quantitative analysis in scattering studies (e.g. Roth & Korn 1993).

Fig. 2 shows time responses in an exponential medium with $a = 214.5$ m for incidence of plane shear waves. Scattered P and S waves develop from the plane shear waves by interference of the random heterogeneities in the medium. The P scattered phases have faster wave speeds than S waves, and are thus recorded before the primary waves in the time response. Strong S coda waves follow the primary waves, and a multiscattering effect enables a long temporal duration of the coda.

The results from four differently realized models are compared with theoretical attenuation curves of eq. (6) in Fig. 3. The attenuation rates in random media (von Karman, exponential, Gaussian) with $a = 214.5$ m are measured consistently despite the change in appearance of the media. The consistency looks weakened with increase of the correlation length of the media since multiple scattering becomes strong (e.g. Frankel & Clayton 1986) and also the log scale in the vertical axis (Q_S^{-1}/ϵ^2) magnifies small differences. As a result, the numerical results from all stochastic random models are well fitted to the range between the theoretical curves with minimum scattering angles (θ_{min}^{SS}) of 60° and 90°. The presented minimum scattering angles accord with those of P waves in a previous study (Hong & Kennett 2003a). It is worth noting a recent report that normalized scattering attenuation rates (Q^{-1}/ϵ^2) reduce with perturbation strength (ϵ) due to the development of coherent
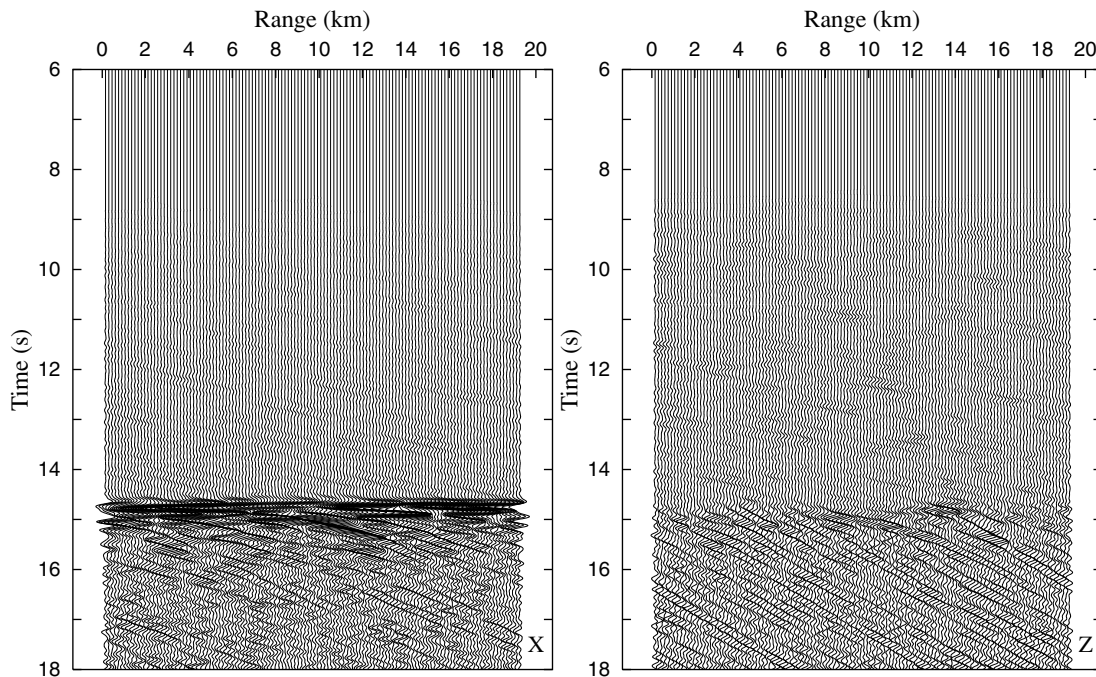

Figure 2. Time responses of S-wave propagation in a von Karman random medium with $\nu = 0.5$ and $a = 214.5$ m. One hundred and twenty-eight receivers are deployed at a distance of 55.9 km from the source position of the plane shear wave. The incident S waves are polarized in the direction of the x-axis and propagate vertically. Major primary waves are observed in the x component, and scattered P phases propagate faster before the primary S waves. A strong S coda develops after the primary waves in both x and z components.
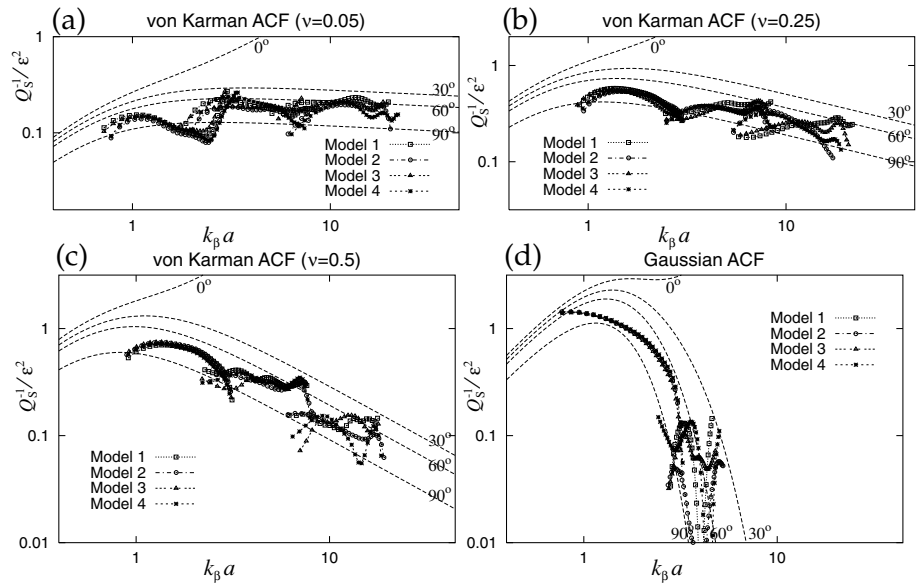
Figure 3. Comparisons of theoretical and numerically estimated scattering attenuation rates of shear waves (Q_S^{-1}) as a function of normalized wavenumber $k_\beta a$ in von Karman random media with Hurst number (a) $\nu = 0.05$, (b) 0.25 and (c) 0.5 (corresponding to the exponential random media) and (d) in a Gaussian random medium. The scattering attenuation rates are well represented by the theoretical curves for a 60–90° minimum scattering angle.

scattered waves which degrade the random nature of the scattering (Hong *et al.* 2003). Thus, the minimum scattering angle can be determined as small at low perturbation strengths. We present the scattering attenuation ratios based on the minimum scattering angle obtained from this study in the following section, but the approach can easily be extended for different perturbation cases.

4 SCATTERING ATTENUATION RATIO OF ELASTIC WAVES

4.1 General pattern

In order to give a detailed description of the variation of scattering attenuation ratios, we use the theoretical expressions for scattering attenuation for *P* and *S* waves in eqs (1) and (6) with the minimum scattering angles resolved in the previous section. This approach will allow investigation of scattering attenuation in various cases without implementation of massive numerical modelling. Note that field data are often analysed in terms of frequency (f) since this analysis does not require comprehension of the detailed seismic properties of the medium. Thus, we focus on the variation of scattering attenuation ratio with frequency, and this will allow direct comparison with field observations. The scattering attenuation rates depend on the velocity ratio (γ) of the medium, and we implement a representative velocity ratio of 1.75 considering plausible crustal velocities of $\alpha_0 = 6.738$ km s^{-1} and $\beta_0 = 3.85$ km s^{-1} (Kennett *et al.* 1995).

Using a simple relationship $f = k_\beta \beta_0/(2\pi) = k_\alpha \alpha_0/(2\pi)$, the theoretical scattering attenuation expressions in eqs (1) and (6) can be rewritten easily as a function of normalized frequency (fa). Note that the variable ka in the theoretical expressions has a one-to-one match to the variable fa for a given velocity set. Thus, the expression with fa is expected to preserve the properties of the theoretical expressions for ka. The implementation of a different velocity set with the same velocity ratio (γ) causes just a relative shift of fa values. For instance, the pattern of theoretical attenuation ratios for a velocity set of $\alpha_0 = 6.738$ km s^{-1} and $\beta_0 = 3.85$ km s^{-1} is held for a set of $\alpha_0 = 4.0$ km s^{-1} and $\beta_0 = 2.286$ km s^{-1}. The dimension of the normalized frequency corresponds to velocity.

In Fig. 4, *S* waves display more attenuation than *P* waves at low fa (<1 km s^{-1}) in all random models. On the other hand, the *P*-wave attenuation becomes comparable or dominant at large fa (>1 km s^{-1}). Also, the *P*-wave attenuation is strengthened in the high-frequency regime with increase in the Hurst number in von Karman media. The relative variation between *P*- and *S*-wave attenuation at high frequencies ($fa > 1$ km s^{-1}) agrees with regional observations (e.g. Castro *et al.* 1997) which display a constant difference between the levels of attenuation.

Scattering attenuation ratios of *P* and *S* waves (Fig. 5) are proportional to fa in a range of $0.1 < fa < 10$ km s^{-1}, and are determined as constant for both of the end regimes (i.e. $fa \gg 10$ km s^{-1}, $fa \ll 0.1$ km s^{-1}). The amplitudes of the constant ratios in the low-frequency limit ($fa \ll 0.1$ km s^{-1}) depend only on the size of the minimum scattering angle, and are 0.34 for $\theta_{\min} = 60°$ and 0.29 for 90°. On the other hand, the ratios at the high-frequency limit ($fa \gg 10$ km s^{-1}) are dependent on both the minimum scattering angle and the type of medium. In particular, the level of the attenuation ratios in von Karman media in the high-frequency regime are proportional to the Hurst number (see also Table 1). On the other hand, the attenuation ratios in Gaussian media display a drastic variation at $fa > 1$ km s^{-1}. The drastic variation in the high-frequency regime is related to the texture of Gaussian media. Since Gaussian media lack a frequency structures in the texture (see Fig. 1), high-frequency waves are scarcely affected by the random heterogeneities in the media. Thus, the consideration of attenuation ratio
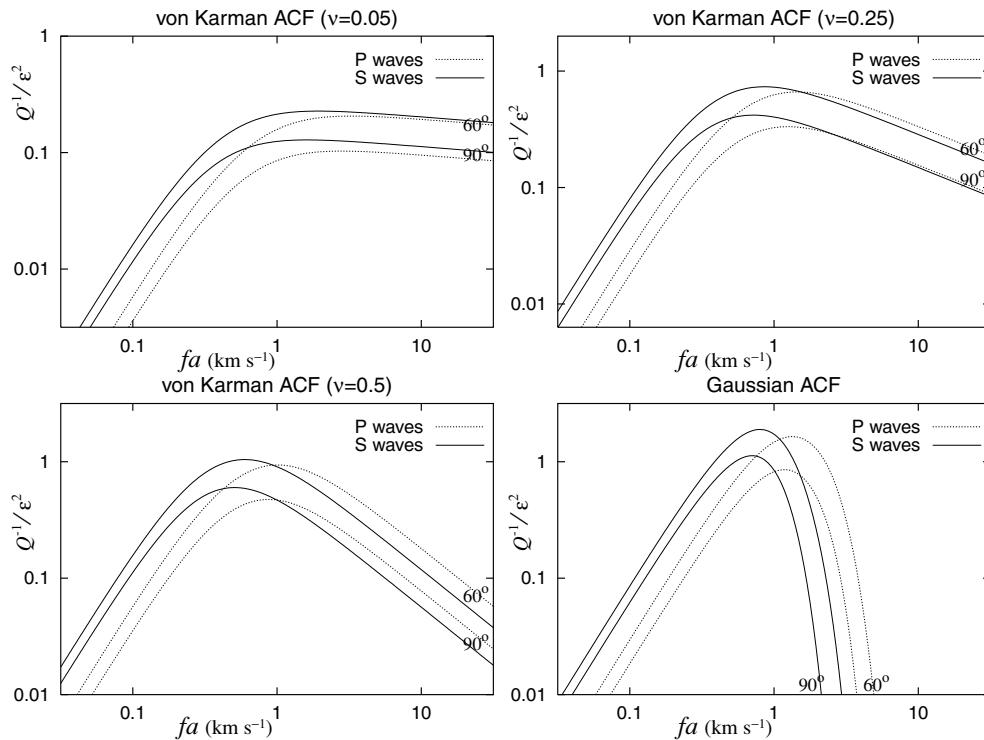
Figure 4. Comparisons of *P* and *S* wave scattering attenuation rates as a function of normalized frequency (*fa*) in von Karman type random media with Hurst number $\nu = 0.05$, 0.25, 0.5 and in a Gaussian random medium, when $\alpha_0 = 6.738$ km s^{-1} and $\beta_0 = 3.85$ km s^{-1} ($\gamma = 1.75$).
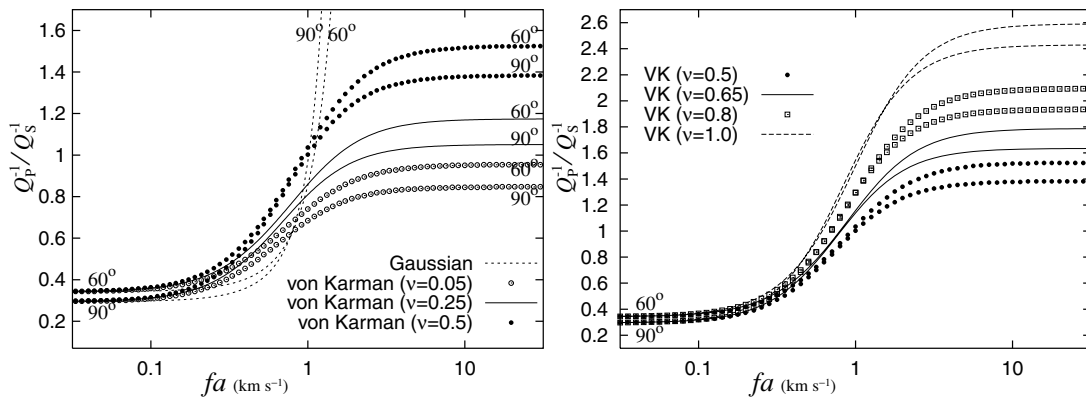

Figure 5. Scattering attenuation ratios of *P* and *S* waves as a function of normalized frequency (*fa*) in von Karman type random media with Hurst number $\nu = 0.05$, 0.25, 0.5 and in a Gaussian random medium, when $\alpha_0 = 6.738$ km s^{-1} and $\beta_0 = 3.85$ km s^{-1} ($\gamma = 1.75$).

in the high-frequency regime is physically meaningless. Therefore, in the sense of characterization of media in terms of stochastic random heterogeneities, von Karman type models which can cover a broad frequency range look to be more reasonable for the representation of media in the Earth than Gaussian models.

The pattern of variation of attenuation ratios in Fig. 5 agrees well with the reported field observations, which vary from 0.4 to 2.9 (Fig. 6). Anderson *et al.* (1965) reported a constant attenuation ratio of 0.44 by analysing low-frequency ($f < 0.02$ Hz) seismic waves. Later, Taylor *et al.* (1986) reported that the ratios increase from 0.5 to 2 with frequency in North America in the frequency range of 0.05 to 3 Hz, and other studies with similar variation patterns have followed in various regions (e.g. Butler *et al.* 1987). In high-frequency ranges ($f > 10$ Hz), the attenuation ratios in the crust and the upper mantle have been reported in various studies to be 1.12 to 2.94 (e.g. Modiano & Hatzfeld 1982; Carpenter & Sanford 1985; Yoshimoto *et al.* 1993; Castro *et al.* 1997).

Taking account of the inclusion of the intrinsic attenuation and different elastic properties (e.g. velocity ratio γ) in the field results, the theoretical scattering attenuation ratios of stochastic media look very reasonable for the description of the heterogeneous nature of the Earth. In fact, most of the field results can be fit to the theoretical curves for von Karman media through implementation of appropriate Hurst numbers and correlation lengths. Occasionally, the theoretical attenuation ratios have less conformity with some field observations

Table 1. Maximum attenuation ratios ($R_Q = Q_P^{-1}/Q_S^{-1}$) for fa in von Karman type media with a different Hurst number (ν) when $\alpha_0 = 6.74$ km s^{-1} and $\beta_0 = 3.85$ km s^{-1} ($\gamma = 1.75$). The ratios are measured at $fa = 100$ km s^{-1}.

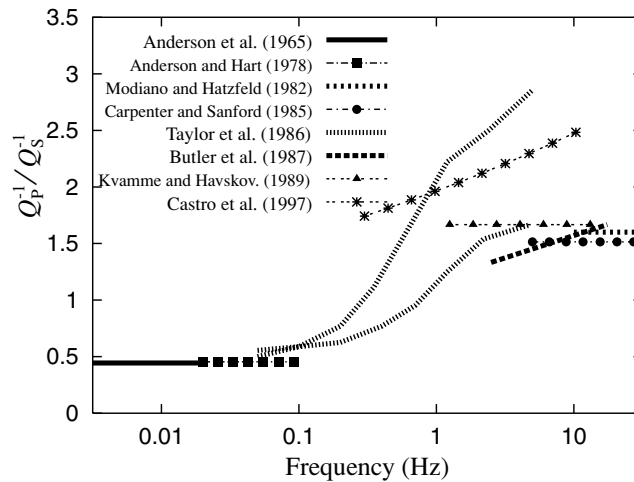| ν	$\theta_{\min}$	$R_Q|_{(fa=100)}$
0.05	60°	0.95
	90°	0.85
0.25	60°	1.17
	90°	1.05
0.5	60°	1.53
	90°	1.38
0.65	60°	1.79
	90°	1.63
0.8	60°	2.10
	90°	1.94
1.0	60°	2.59
	90°	2.43

Figure 6. Apparent attenuation ratios of *P* and *S* waves observed in various areas (see also, Fig. 5.3 in Sato & Fehler 1998). The variation of the attenuation ratios with frequency is close to the pattern in theoretical attenuation ratios in Fig. 5.

(e.g. Yoshimoto *et al.* 1993, 1998) where the intrinsic attenuation is dominant and independent of the scattering attenuation. For instance, the intrinsic attenuation in the Kanto area (see, Yoshimoto *et al.* 1993) is about twice the scattering attenuation and varies independently with frequency from the scattering attenuation variation (Fehler *et al.* 1992).

4.2 Effect of density perturbation and velocity ratio

The Earth is composed of various materials, and consequently has varying influences on the scattering of seismic waves. We examine the effect of other factors on the scattering attenuation ratios of *P* and *S* waves. As shown in the theoretical expressions in eqs (1) and (6), the other parameters which can change the level of attenuation ratios are the density perturbation (K) and the velocity ratio (γ).

First, we consider three additional different levels of density perturbation: $K = 0$, 0.4 and 1.0, where K is the constant controlling the density perturbation in eq. (9). The $K = 0$ density perturbation represents a case when there is no density perturbation, and $K = 1.0$ is for a case when the density perturbation is as high as the velocity perturbation.

The form of variation of the attenuation ratio is held despite the change in the level of density perturbation (see, Fig. 7). The relative variation of attenuation ratios at the low-frequency limit is very weak compared with that in the high-frequency regime, and the influence of density perturbation is negligible at the low-frequency limit. The attenuation ratios for $\theta_{\min} = 60°$ are rarely changed for the variation of density perturbation, while those for $\theta_{\min} = 90°$ decrease slightly with K. This implies that the density perturbation does not produce a noticeable relative variation in *P*- and *S*-wave attenuation rates at small scattering angles ($\leq 60°$). However, in the large-angle regime ($>60°$), *S*-wave scattering is expected to increase significantly with the density perturbation strength compared with *P*-wave scattering, since the *S* waves are polarized perpendicularly to the incidence direction and the energy concentrates around the polarization direction.
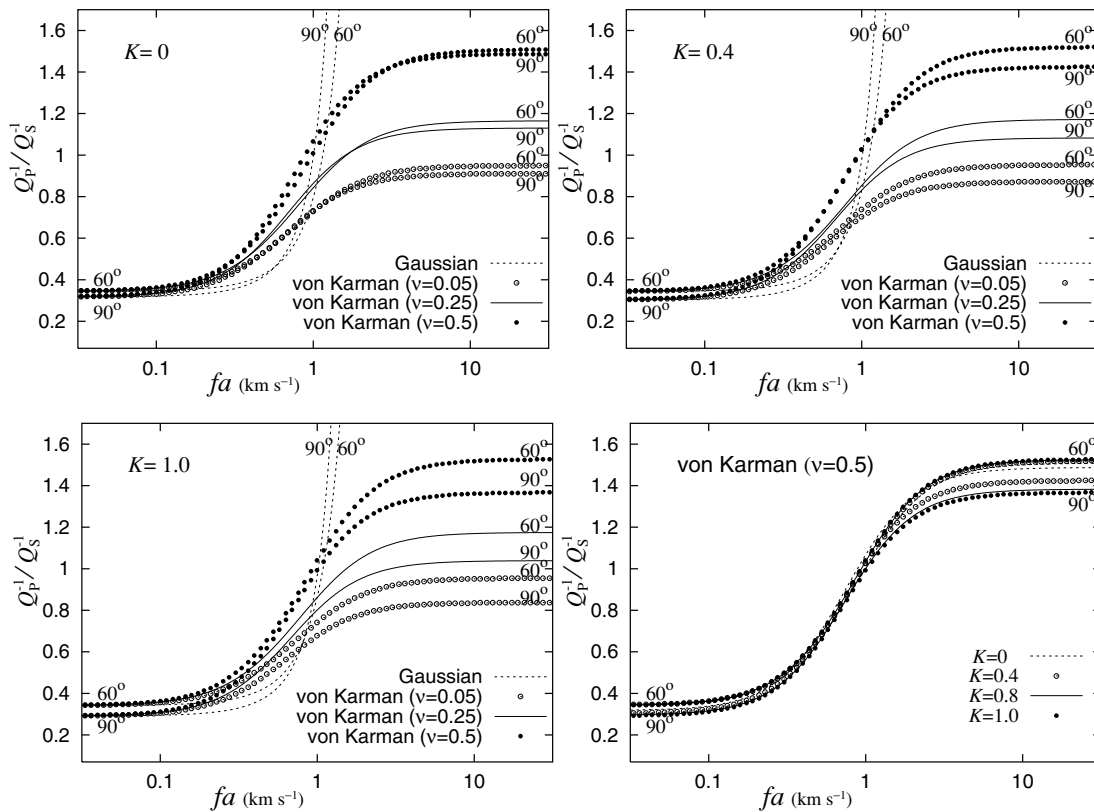
Figure 7. Scattering attenuation ratios as a function of *fa* for various density perturbations and the representative variation in a von Karman medium with $\nu = 0.5$. The attenuation ratios for *fa* are not much affected by the density perturbation, but the density perturbation slightly strengthens the shear wave scattering in the high-frequency regime (*fa* > 1).

The density perturbation amplifies scattering in the direction of polarization, thus the relative variation of attenuation ratios is prominent at a large minimum scattering angle. The overall influence of the density perturbation on attenuation ratios, however, is rather trivial considering the difference in the levels of attenuation ratios between different types of media. As a result, velocity perturbation appears to play a dominant role in the determination of scattering attenuation ratios.

We now investigate the effect of the velocity ratio on the scattering attenuation ratios. Considering the velocity structure of the Earth allowing shear wave scattering, we implement seven additional velocity ratios ($\gamma = 1.55, 1.6, 2.0, 2.5, 3.0, 4.0$ and 8.0). Note that the extreme velocity ratios for elastic materials can be given by $\sqrt{2}$ (when $\lambda = 0$) and ∞ (when $\beta = 0$). For comparison, we set the *P*-wave velocity constant (6.738 km s^{-1}), and adapt *S*-wave velocity following the velocity ratios.

The overall variation pattern of attenuation ratios is held despite the change in velocity ratio. However, the level of attenuation ratios varies with the velocity ratio. Attenuation ratios are inversely proportional to velocity ratio in the low-frequency regime ($fa \ll 0.1$). The attenuation ratios display a complex dependence on the velocity ratio in the high-frequency regime: the level of the attenuation ratio is proportional to the velocity ratio when $fa > 2.5$, but decreases with velocity ratio when $fa < 2.5$ (Fig. 8). The level of the attenuation ratio is also dependent on the type of medium in the high-frequency regime. In particular, the level increases with the Hurst number of von Karman media.

5 DISCUSSION AND CONCLUSIONS

The nature of scattering attenuation ratios (Q_P^{-1}/Q_S^{-1}) of elastic waves in stochastic random media has been investigated by using theoretical expressions for attenuation based on the first-order Born approximation. The theoretical expressions were compared with results from numerical modelling. The numerical results are well fitted to the theoretical curves with a minimum scattering angle of 60–90° for media with a mild perturbation strength (10 per cent velocity perturbation). The scattering attenuation ratios for normalized frequency (*fa*) are highly dependent on the type of medium and the velocity ratio (γ). The discernible difference in the level of attenuation ratios with frequency allows prompt use of field observation for the characterization of media. The scattering attenuation ratios are rarely affected by density perturbation but mainly by velocity perturbation, velocity ratio and the type of medium.

Considering the reported field observations, von Karman models look suitable for the representation of small-scale heterogeneities in the Earth; von Karman models can satisfy a wide level of variation in attenuation ratios through implementation of an appropriate Hurst number and correlation length. In particular, Hurst numbers larger than 0.5 (e.g. Saito *et al.* 2003) need to be implemented for the description of heterogeneities at some regions. On the other hand, the Gaussian model represents the extreme case of low-frequency textured media, so
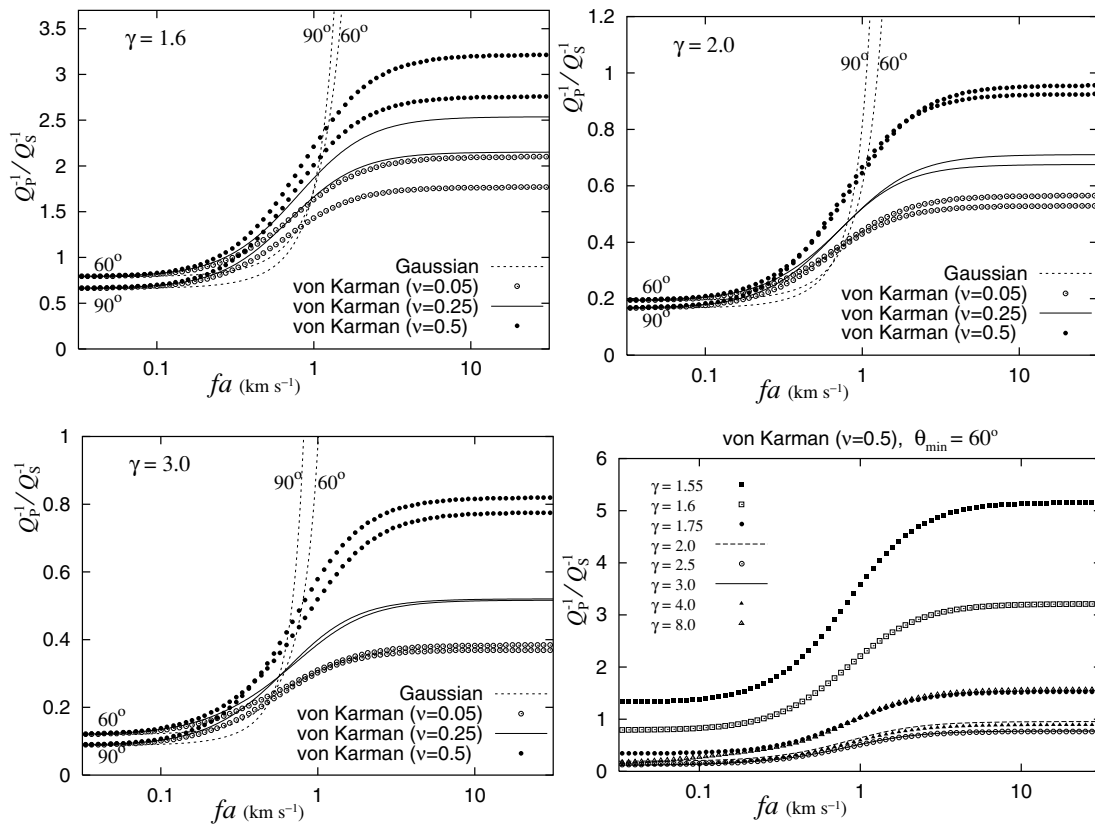
Figure 8. Scattering attenuation ratios as a function of *fa* for various velocity ratios ($\gamma = 1.55$, 1.6, 1.75, 2.0, 2.5, 3.0, 4.0 and 8.0), and a representative variation in a von Karman medium with $\nu = 0.5$ and $\theta_{min} = 60°$. The level of the attenuation ratios are highly dependent on the velocity ratio, and in general increase with decrease of the velocity ratio.

it does not support investigation through attenuation ratios in the high-frequency regime. The Gaussian models look inappropriate for the description of heterogeneities with a large correlation length, especially in problems with high-frequency incident waves. It is expected that the scattering attenuation ratios can be implemented for the characterization of media in the Earth through comparison between theoretical variation and field observation. The determined stochastic model could ultimately be extended to aid understanding of the seismic signature in the Earth.

It is noteworthy that the theoretical expressions of the current work are developed in the context of the Born approximation which may fail in the high-frequency regime (Weaver 1990). The theoretical expressions for attenuation, however, were examined with numerical results in a range up to $ka = 15$ in this study and a previous work (Hong & Kennett 2003a), and the attenuation ratios retain validity up to such range. Moreover, since the attenuation ratios in the high-frequency regime ($fa > 3$) are determined constant, it is also possible to use the attenuation ratios in the high-frequency regime as long as the media are statistically randomly heterogeneous.

In general, the intrinsic attenuation in the Earth is related to the physical and chemical nature of the various media, for instance rock type (Assefa *et al.* 1999), material state (Del Pezzo *et al.* 1995), temperature (Roth *et al.* 2000), thermoelasticity (Aki 1980; Frankel *et al.* 1990), variation of material composition with depth (e.g. Tselentis 1993; Menke *et al.* 1995; Der 1998; Flanagan & Wiens 1998) and tectonic activity (Frankel *et al.* 1990; Sarker & Abers 1998). Naturally, this physical and chemical variation can cause perturbation in the media and an increase in scattering in the seismic wavefield. The variation of theoretical scattering attenuation ratios presented in this study is very close to the apparent attenuation ratios of field observation in many areas. This feature supports the idea that scattering attenuation ratios can be implemented as a reference parameter for the characterization of media in the Earth. Further, it is expected that we can resolve small-scale heterogeneities in the crust using scattering attenuation ratios.

However, some properties, for example frequency dependence (Hatzidimitriou 1994; Akinci & Eyidoğan 2000), of intrinsic attenuation are different from those of scattering attenuation. Also, it has been reported that attenuation rates may vary with the propagation distance in a zone with an anisotropic distribution of heterogeneities (e.g. Campillo & Plantet 1991; Tselentis 1993; Menke *et al.* 1995). Thus, in the next stage of work it is necessary to develop theoretical expressions for attenuation and numerical models combining scattering and intrinsic attenuation in order to understand high-frequency seismic attenuation in the crust. Also, variation in seismic attenuation during propagation through layered media should help in understanding the the attenuation of seismic waves in the Earth.

ACKNOWLEDGMENTS

REFERENCES

Adams, D.A. & Abercrombie, R.E., 1998. Seismic attenuation above 10 Hz in southern California from coda wave recorded in the Cajon Pass borehole, *J. geophys. Res.,* **103,** 24 257–24 270.

Aki, K., 1980. Attenuation of shear-waves in the lithosphere for frequencies from 0.05 to 25 Hz, *Phys. Earth planet. Inter.,* **21,** 50–60.

Aki, K. & Richards, P.G., 1980. *Quantitative Seismology, Theory and Methods,* Vol. 1, W.H. Freeman, San Francisco.

Akinci, A. & Eyidoğan, H., 2000. Scattering and anelastic attenuation of seismic energy in the vicinity of north Anatolian fault zone, eastern Turkey, *Phys. Earth planet. Inter.,* **122,** 229–239.

Anderson, D.L., Ben-Menahem, A. & Archambeau, C.B., 1965. Attenuation of seismic energy in the upper mantle, *J. geophys. Res.,* **70,** 1441–1448.

Assefa, S., McCann, C., & Sothcott, J., 1999. Attenuation of *P*- and *S*-waves in limestones, *Geophys. Prospect.,* **47,** 359–392.

Butler, R., McCreery, C.S., Frazer, L.N. & Walker, D.A., 1987. High-frequency seismic attenuation of oceanic *P* and *S* waves in the western Pacific, *Geophys. J. Res.,* **92**(B2), 1383–1396.

Campillo, M. & Plantet, J.L., 1991. Frequency dependence and spatial distribution of seismic attenuation in France: experimental results and possible interpretations, *Phys. Earth planet. Inter.,* **67,** 48–64.

Carpenter, P.J. & Sanford, A.R., 1985. Apparent *Q* for upper crustal rocks of the Central Rio Grande Rift, *J. geophys. Res.,* **90,** 8661–8674.

Castro, R.R., Rebollar, C.J., Inzunza, L., Orozco, L., Sánchez, J., Gálvez, O., Farfán, F.J. & Méndez, I., 1997. Direct body-wave *Q* estimates in northern Baja California, Mexico, *Phys. Earth planet. Inter.,* **103,** 33–38.

Chung, T.-W. & Sato, H., 2001. Attenuation of high-frequency *P* and *S* waves in the crust of southeastern South Korea, *Bull. seism. Soc. Am.,* **91,** 1867–1874.

Del Pezzo, E., Ibanez, J., Morales, J., Akinci, A. & Maresca, R., 1995. Measurement of intrinsic and scattering seismic attenuation in the crust, *Bull. seism. Soc. Am.,* **85,** 1373–1380.

Der, Z.A., 1998. High-frequency *P*- and *S*-wave attenuation in the Earth, *Pure appl. Geophys.,* **153,** 273–310.

Fang, Y. & Müller, G., 1996. Attenuation operators and complex wave velocities for scattering in random media, *Pure appl. Geophys.,* **148,** 269–285.

Fehler, M., Hoshiba, M., Sato, H. & Obara, K., 1992. Separation of scattering and intrinsic attenuation for the Kanto-Tokai region, Japan, using measurements of *S*-wave energy versus hypocentral distance, *Geophys. J. Int.,* **108,** 787–800.

Flanagan, M.P. & Wiens, D.A., 1998. Attenuation of broadband *P* and *S* waves in Tonga: observations of frequency dependent *Q*, *Pure appl. Geophys.,* **153,** 345–375.

Frankel, A. & Clayton, R.W., 1986. Finite difference simulations of seismic scattering: implications for the propagation of short-period seismic waves in the crust and models of crustal heterogeneities, *J. geophys. Res.,* **91**(B6), 6465–6489.

Frankel, A., McGarr, A., Bicknell, J. Mori, J., Seeber, L. & Cranswick, E., 1990. Attenuation of high-frequency shear waves in the crust: measurements from New York State, South Africa, and southern California, *J. geophys. Res.,* **95,** 17 441–17 457.

Frenje, L. & Juhlin, C., 2000. Scattering attenuation: 2-D and 3-D finite difference simulations vs. theory, *J. appl. Geophys.,* **44,** 33–46.

Hatzidimitriou, P.M., 1994. Scattering and anelastic attenuation of seismic energy in northern Greece, *Pure appl. Geophys.,* **143,** 587–601.

Hatzidimitriou, P.M., 1995. *S*-wave attenuation in the crust in northern Greece, *Bull. seism. Soc. Am.,* **85,** 1381–1387.

Hedlin, M.A. & Shearer, P.M., 2002. Probing mid-mantle heterogeneity using *PKP* coda waves, *Phys. Earth planet. Inter.,* **130,** 195–208.

Hong, T.-K. & Kennett, B.L.N., 2002a. A wavelet-based method for simulation of two-dimensional elastic wave propagation, *Geophys. J. Int.,* **150,** 610–638.

Hong, T.-K. & Kennett, B.L.N., 2002b. On a wavelet-based method for the numerical simulation of wave propagation, *J. Comput. Phys.,* **183,** 577–622.

Hong, T.-K. & Kennett, B.L.N., 2003a. Scattering attenuation of 2-D elastic waves: theory and numerical modelling using a wavelet-based method, *Bull. seism. Soc. Am.,* **93,** 922–938.

Hong, T.-K. & Kennett, B.L.N., 2003b. Modelling of seismic waves in heterogeneous media using a wavelet-based method: application to fault and subduction zones, *Geophys. J. Int.,* **154,** 483–498.

Hong, T.-K., Kennett, B.L.N & Wu, R.-S., 2003. Factors affecting the evaluation of scattering attenuation, *EOS, Trans. Am. geophys. Un.,* **84**(47), Fall Meeting Supplement, abstract S22B–0460.

Jannaud, L.R., Adler, P.M., Jacquin, C.G., 1991. Frequency dependence of the *Q* factor in random media, *J. geophys. Res.,* **96,** 18 233–18 243.

Kennett, B.L.N., Engdahl, E.R. & Buland, R., 1995. Constraints on seismic velocities in the Earth from travel times, *Geophys. J. Int.,* **122,** 108–124.

Line, C.E.R., Hobbs, R.W., Hudson, J.A. & Synder, D.B., 1998. Statistical inversion of controlled-source seismic data using parabolic wave scattering theory, *Geophys. J. Int.,* **132,** 61–78.

Mayeda, K., Koyanagi, S., Hoshiba, M., Aki, K. & Zeng, Y., 1992. A comparative study of scattering, intrinsic, and coda Q^{-1} for Hawaii, Long Valley, and central California between 1.5 and 15.0 Hz, *J. geophys. Res.,* **97,** 6643–6659.

Menke, W., Levin, V. & Sethi, R., 1995. Seismic attenuation in the crust at the mid-Atlantic plate boundary in south-west Iceland, *Geophys. J. Int.,* **122,** 175–182.

Modiano, T. & Hatzfeld, D., 1982. Experimental study of the spectral content for shallow earthquakes, *Bull. seism. Soc. Am.,* **72,** 1739–1758.

Roth, M. & Korn, M., 1993. Single scattering theory versus numerical modelling in 2-D random media, *Geophys. J. Int.,* **112,** 124–140.

Roth, E.G., Wiens, D.A. & Zhao, D., 2000. An empirical relationship between seismic attenuation and velocity anomalies in the upper mantle, *Geophys. Res. Lett.,* **27,** 601–604.

Saito, T., Sato, H., Fehler, M. & Ohtake, M., 2003. Simulating the envelope of scalar waves in 2D random media having power-law spectra of velocity fluctuation, *Bull. seism. Soc. Am.,* **93,** 240–252.

Sarker, G. & Abers, G.A., 1998. Comparison of seismic body wave and coda wave measures of *Q*, *Pure appl. Geophys.,* **153,** 665–683.

Sato, H., 1982. Amplitude attenuation of impulsive waves in random media based on travel time corrected mean wave formalism, *J. acoust. Soc. Am.,* **71,** 559–564.

Sato, H. & Fehler, M., 1998. *Seismic Wave Propagation and Scattering in the Heterogeneous Earth,* Springer, New York.

Shapiro, S.A. & Kneib, G., 1993. Seismic attenuation by scattering: theory and numerical results, *Geophys. J. Int.,* **114,** 373–391.

Shiomi, K., Sato, H. & Ohtake, M., 1997. Broadband power-law spectra of well-log data in Japan, *Geophys. J. Int.,* **130,** 57–64.

Taylor, S.R., Bonner, B.P. & Zandt, G., 1986. Attenuation and scattering of broadband *P* and *S* waves across North America, *J. geophys. Res.,* **91,** 7309–7325.

Tselentis, G., 1993. Depth-dependent seismic attenuation in Western Greece, *Tectonophysics,* **225,** 523–528.

Tselentis, G., 1998. Intrinsic and scattering seismic attenuation in W. Greece, *Pure appl. Geophys.,* **153,** 703–712.

Weaver, R.L., 1990. Diffusivity of ultrasound in polycrystals, *J. Mech. Phys. Solids*, **38**(1), 55–86.

Wu, R.-S., 1982. Attenuation of short period seismic waves due to scattering, *Geophys. Res. Lett.*, **9**, 9–12.

Yoshimoto, K., Sato, H. & Ohtake, M., 1993. Frequency-dependent atten-

uation of *P* and *S* waves in the Kanto area, Japan, based on the coda-normalization method, *Geophys. J. Int.*, **114**, 165–174.

Yoshimoto, K., Sato, H., Iio, Y., Ito, H., Ohminato, T. & Ohtake, M., 1998. Frequency-dependent attenuation of high-frequency *P* and *S* waves in the upper crust in western Nagano, Japan, *Pure appl. Geophys.*, **153**, 489–502.

APPENDIX A: DERIVATION OF *S*-WAVE SCATTERING ATTENUATION RATES

Following the procedure for the derivation of *P*-wave scattering attenuation in Hong & Kennett (2003a), we formulate the scattering attenuation rates of *S* waves (Q_S^{-1}) as a function of normalized wavenumber ($k_\beta a$) in 2-D random heterogeneous media.

We first consider that the wavefield (u_j, $j = x, z$) is composed of primary waves (u_j^0, $j = x, z$) and scattered waves (u_j^s, $j = x, z$). Then the primary waves in 2-D elastic media satisfy the relationships

$$\rho_0 \frac{\partial^2 u_x^0}{\partial t^2} = \frac{\partial \sigma_{xx}^0}{\partial x} + \frac{\partial \sigma_{xz}^0}{\partial z}, \qquad \rho_0 \frac{\partial^2 u_z^0}{\partial t^2} = \frac{\partial \sigma_{xz}^0}{\partial x} + \frac{\partial \sigma_{zz}^0}{\partial z}, \tag{A1}$$

where

$$\sigma_{xx}^0 = (\lambda_0 + 2\mu_0)\frac{\partial u_x^0}{\partial x} + \lambda_0 \frac{\partial u_z^0}{\partial z}, \qquad \sigma_{zz}^0 = \lambda_0 \frac{\partial u_x^0}{\partial x} + (\lambda_0 + 2\mu_0)\frac{\partial u_z^0}{\partial z},$$

$$\sigma_{xz}^0 = \mu_0 \left(\frac{\partial u_x^0}{\partial z} + \frac{\partial u_z^0}{\partial x} \right), \tag{A2}$$

λ_0 and μ_0 are Lamé coefficients and ρ_0 is the density of the background medium.

When the vertically incident (*z*-axis direction) and horizontally polarized (*x*-axis direction) plane *S* waves (Fig. A1) are considered as the primary waves, they are given by

$$u_x^0 = e^{i(k_\beta z - \omega t)}, \qquad u_z^0 = 0, \tag{A3}$$

where ω is the angular frequency. The scattered waves can be represented using body forces f_j^s ($j = x, z$ or 1, 2) for the scattering effects from the perturbation of physical parameters. Thus, the body forces f_j^s can be computed by using (A1) and (A3), and they are written in terms of the primary waves and the fractional fluctuation of physical parameters as

$$f_x^s = -\left(k_\beta^2 (\delta\rho\beta_0^2 - \delta\mu) + i k_\beta \frac{\partial}{\partial z}(\delta\mu) \right) u_x^0, \qquad f_z^s = -i k_\beta \frac{\partial}{\partial x}(\delta\mu) u_x^0. \tag{A4}$$

Using the empirical relationship (9) between physical parameters, eq. (A4) can be rewritten in terms of the fractional fluctuation term $\xi(x, z)$ as
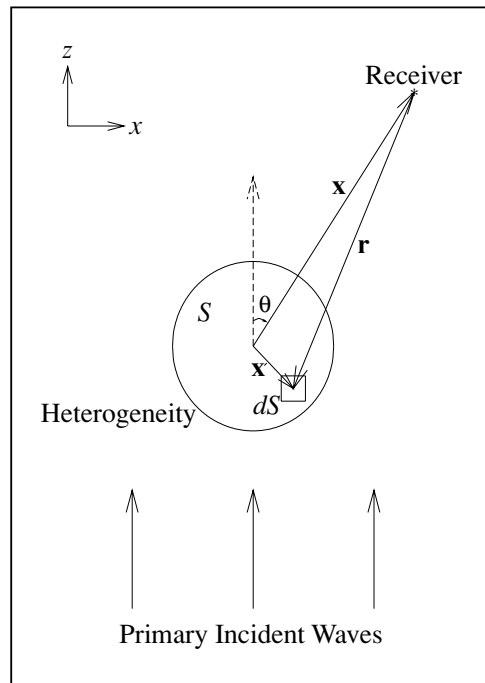

Figure A1. The scattering of the primary incident waves at the scatterer $d\mathsf{S}$, a part of the whole heterogeneous area S. θ is the scattering angle from the incident direction of primary waves along the *z*-axis. $\mathbf{x}$, $\mathbf{x}'$ are the location vectors for the receiver and a scatterer. $\mathbf{r}$ links the scatterer to the receiver.

$$f_x^s = -k_\beta \beta_0^2 \rho_0 \left(k_\beta C_1^S \xi + i C_2^S \frac{\partial \xi}{\partial z} \right) \exp[i(k_\beta z - \omega t)],$$

(A5)

$$f_z^s = -i k_\beta \beta_0^2 \rho_0 C_2 \frac{\partial \xi}{\partial x} \exp[i(k_\beta z - \omega t)],$$

where C_1^S and C_2^S are constants given by

$$C_1^S = -2, \quad C_2^S = K + 2.$$

(A6)

Hereafter we use symbols without the subscript 0 representing the background medium for simplicity in mathematical expressions.

Displacement fields, generated by body forces (f_k^s, $k = x, z$ or 1, 2) which are induced by perturbation of physical properties, can be expressed using the Green's function $\overline{G}_{jk}(\mathbf{x}, \mathbf{x}')$ by

$$u_j^s(\mathbf{x}) = \sum_{k=1}^{2} \int_S f_k^s(\mathbf{x}') \overline{G}_{jk}(\mathbf{x}, \mathbf{x}') \, dS(\mathbf{x}'), \quad j = 1, 2,$$

(A7)

where S is the inhomogeneity area. The far-field Green's functions of 2-D elastic waves are given by (Hong & Kennett 2003a)

$$\begin{pmatrix} \overline{G}_{12}^P \\ \overline{G}_{22}^P \end{pmatrix} = \frac{i}{4\alpha^2 \rho} \sqrt{\frac{2}{\pi k_\alpha |\mathbf{x}|}} \exp\left[i \left(k_\alpha |\mathbf{x}| - k_\alpha \mathbf{n} \cdot \mathbf{x}' - \frac{\pi}{4} \right) \right] \begin{pmatrix} \sin\theta \cos\theta \\ \cos^2\theta \end{pmatrix},$$

(A8)

and

$$\begin{pmatrix} \overline{G}_{12}^S \\ \overline{G}_{22}^S \end{pmatrix} = \frac{i}{4\beta^2 \rho} \sqrt{\frac{2}{\pi k_\beta |\mathbf{x}|}} \exp\left[i \left(k_\beta |\mathbf{x}| - k_\beta \mathbf{n} \cdot \mathbf{x}' - \frac{\pi}{4} \right) \right] \begin{pmatrix} -\sin\theta \cos\theta \\ \sin^2\theta \end{pmatrix}.$$

(A9)

We now obtain the far-field scattered wavefields as

$$u_j^{SP} = \sqrt{\frac{k_\alpha}{\gamma^2 8\pi |\mathbf{x}|}} \exp\left[-i \left(\omega t - k_\alpha |\mathbf{x}| + \frac{\pi}{4} \right) \right] \cdot \left(-i k_\beta C_1^S A_{j1}^P(\theta) \int_S \xi e^{ik_\alpha(\gamma z - \mathbf{n} \cdot \mathbf{x}')} \, dS(\mathbf{x}') \right.$$

$$\left. + C_2^S A_{j1}^P(\theta) \int_S \frac{\partial \xi}{\partial z} e^{ik_\alpha(\gamma z - \mathbf{n} \cdot \mathbf{x}')} \, dS(\mathbf{x}') + C_2^S A_{j2}^P(\theta) \int_S \frac{\partial \xi}{\partial x} e^{ik_\alpha(\gamma z - \mathbf{n} \cdot \mathbf{x}')} \, dS(\mathbf{x}') \right),$$

(A10)

and

$$u_j^{SS} = \sqrt{\frac{k_\beta}{8\pi |\mathbf{x}|}} \exp\left[-i \left(\omega t - k_\beta |\mathbf{x}| + \frac{\pi}{4} \right) \right] \cdot \left(-i k_\beta C_1^S A_{j1}^S(\theta) \int_S \xi e^{ik_\beta(z - \mathbf{n} \cdot \mathbf{x}')} \, dS(\mathbf{x}') \right.$$

$$\left. + C_2^S A_{j1}^S(\theta) \int_S \frac{\partial \xi}{\partial z} e^{ik_\beta(z - \mathbf{n} \cdot \mathbf{x}')} \, dS(\mathbf{x}') + C_2^S A_{j2}^S(\theta) \int_S \frac{\partial \xi}{\partial x} e^{ik_\beta(z - \mathbf{n} \cdot \mathbf{x}')} \, dS(\mathbf{x}') \right),$$

(A11)

where A_{ij}^k ($i, j = 1, 2, k = P, S$) is given in (5). Using the partial integration for the partial differentials of ξ in (A10) and (A11) and considering the scattered P and S waves in a single component (radial or tangential) by rotation of the coordinate axes (e.g. Sato & Fehler 1998), we obtain

$$u_r^{SP} = \sin\theta u_x^{SP} + \cos\theta u_z^{SP}$$

$$= i \sqrt{\frac{k_\alpha^3}{\gamma^2 8\pi |\mathbf{x}|}} C_r^S(\theta) \exp\left[-i \left(\omega t - k_\alpha |\mathbf{x}| + \frac{\pi}{4} \right) \right] \int_S \xi e^{ik_\alpha(\gamma z - \mathbf{n} \cdot \mathbf{x}')} \, dS(\mathbf{x}'),$$

(A12)

$$u_t^{SS} = \cos\theta u_x^{SS} - \sin\theta u_z^{SS}$$

$$= i \sqrt{\frac{k_\beta^3}{8\pi |\mathbf{x}|}} C_t^S(\theta) \exp\left[-i \left(\omega t - k_\beta |\mathbf{x}| + \frac{\pi}{4} \right) \right] \int_S \xi e^{ik_\beta(z - \mathbf{n} \cdot \mathbf{x}')} \, dS(\mathbf{x}'),$$

where $C_r^S(\theta)$ and $C_t^S(\theta)$ are given in (8).

Average scattered energy, which can be measured by the ensemble averages of the displacement terms, is calculated in order to assess the average scattered energy, and is given in a simple form as function of the power spectral density function $\mathcal{P}(k)$ for stochastic random media:

$$\left\langle |u_r^{SP}|^2 \right\rangle = \frac{k_\alpha^3 S}{\gamma^2 8\pi |\mathbf{x}|} \left[C_r^S(\theta) \right]^2 \mathcal{P}\left(k_\alpha \sqrt{1 + \gamma^2 - 2\gamma \cos\theta} \right),$$

$$\left\langle |u_t^{SS}|^2 \right\rangle = \frac{k_\beta^3 S}{8\pi |\mathbf{x}|} \left[C_t^S(\theta) \right]^2 \mathcal{P}\left(2 k_\beta \sin\frac{\theta}{2} \right).$$

(A13)

Since Q_S^{-1} corresponds to the energy loss per unit area divided by wavenumber, we can express Q_S^{-1} in terms of the standard deviation (ϵ) of velocity fluctuation in the 2-D media by

$$\frac{Q_S^{-1}}{\epsilon^2} = \frac{1}{S k_\beta} \int_\theta \left(\frac{\alpha}{\beta} \left\langle |u_r^{SP}|^2 \right\rangle + \left\langle |u_t^{SS}|^2 \right\rangle \right) dA,$$
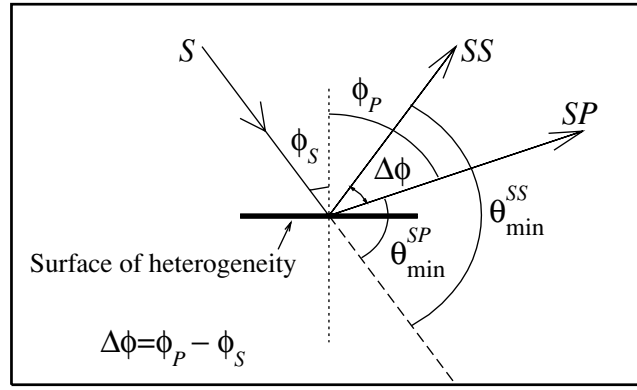
(A14)

Figure A2. Diagram for determining the minimum scattering angle for *S* waves using Snell's law. A specific situation is considered for the determination of θ_{min}^{SP} in terms of θ_{min}^{SS}; the *S* wave is incident with angle ϕ_S on the surface of heterogeneity for the perpendicular axis to the surface and the *SS* scattered waves is reflected on the surface with angle θ_{min}^{SS} for the incident direction (*z*-axis direction in this study). The *SP* scattered wave is reflected on the surface with angle ϕ_P for the perpendicular axis and θ_{min}^{SP} for the incident direction.

where A is the arc length through which scattered waves propagate and therefore dA is given by $r\, d\theta$ (Frankel & Clayton 1986). Note that scaling α/β is applied to $\langle |u_r^{SP}|^2 \rangle$ considering the wave type conversion (Sato & Fehler 1998).

The traveltime correction is considered by neglecting the contribution of forward scattering inside the minimum scattering angle (Sato & Fehler 1998). Since the scattered angles of *SP* and *SS* waves from a heterogeneity are different, we introduce θ_{min}^{SP} for the *P*-wave type scattering and θ_{min}^{SS} for the *S*-wave type scattering. Therefore we can represent the theoretical Q_S^{-1} with the traveltime correction as

$$\frac{Q_S^{-1}}{\epsilon^2} = \frac{r}{Sk_\beta} \left(\gamma \int_{\theta_{min}^{SP}}^{2\pi - \theta_{min}^{SP}} \left\langle |u_r^{SP}|^2 \right\rangle d\theta + \int_{\theta_{min}^{SS}}^{2\pi - \theta_{min}^{SS}} \left\langle |u_t^{SS}|^2 \right\rangle d\theta \right). \tag{A15}$$

When $|\mathbf{x}|$ is large enough, we can assume $|\mathbf{x}| \approx r$. Also, θ_{min}^{SP} can be represented in terms of θ_{min}^{SS} by using Snell's law. When we consider the *SS* scattered waves which are reflected with the minimum scattering angle θ_{min}^{SS} from the boundary of heterogeneity, the corresponding reflection angle of *SP* scattered waves can be calculated using the single scattering idea as (see, Fig. A2)

$$\theta_{min}^{SP} = \theta_{min}^{SS} - \Delta\phi, \tag{A16}$$

where $\Delta\phi = \phi_P - \phi_S$ and ϕ_j $(j = P, S)$ is

$$\phi_S = \frac{\pi - \theta_{min}^{SS}}{2}, \qquad \phi_P = \sin^{-1}(\gamma \sin\phi_S). \tag{A17}$$

Thus, the theoretical scattering variation is given by

$$\frac{Q_S^{-1}}{\epsilon^2} = \frac{k_\beta^2}{8\pi\gamma^4} \int_{\theta_{min}^{SP}}^{2\pi - \theta_{min}^{SP}} \left[C_r^S(\theta) \right]^2 \mathcal{P} \left(\frac{k_\beta}{\gamma} \sqrt{1 + \gamma^2 - 2\gamma\cos\theta} \right) d\theta$$

$$+ \frac{k_\beta^2}{8\pi} \int_{\theta_{min}^{SS}}^{2\pi - \theta_{min}^{SS}} \left[C_t^S(\theta) \right]^2 \mathcal{P} \left(2k_\beta \sin\frac{\theta}{2} \right) d\theta. \tag{A18}$$